



Preparation of an anion dye intercalated into layered double hydroxides and its controllable luminescence properties

Zhiyong Sun, Lan Jin, Wenying Shi, Min Wei*, Xue Duan

State Key Laboratory of Chemical Resource Engineering, Beijing University of Chemical Technology, Beijing 100029, China

ARTICLE INFO

Article history:

Received 24 December 2009

Received in revised form 1 April 2010

Accepted 15 April 2010

Keywords:

ANS

Layered double hydroxide

Intercalation

ANS-LDH composites

Controllable photoluminescence

ABSTRACT

The inorganic–organic composites have been prepared by intercalation of ammonium 1-anilinoanthracene-8-sulfonate (ANS) into ZnAl and MgAl layered double hydroxide (LDH) with the molar ratio (M^{2+}/M^{3+}) of 2:1 and 3:1, respectively. The powder X-ray diffraction (XRD) and Fourier transform infrared spectroscopy (FT-IR) confirm the intercalation of ANS into the galleries of LDH. Fluorescence polarization method was applied to investigate the preferential orientation of the inter-layer ANS molecule, and the results show that ANS anions are accommodated between the sheets of Zn₂Al-LDH, Zn₃Al-LDH, Mg₂Al-LDH and Mg₃Al-LDH with an orientation angle ψ (defined as the angle between the transition moment of ANS molecule with respect to the normal to the LDH layer) of 58°, 57°, 55° and 52°, respectively. TG–DTA results reveal that the thermal stability of ANS was markedly enhanced upon intercalation. Fluorescence spectra demonstrate that the Zn₃Al-ANS-LDH sample exhibits the optimal luminous intensity among the four ANS-LDH composites. It was also found that the luminescence behavior of ANS can be modulated *via* changing the two parameters: the type and ratio of cation species in LDH matrix due to host–guest interactions. Therefore, the ANS-LDH composites can be used as good candidates for solid photoluminescence materials.

© 2010 Elsevier B.V. All rights reserved.

1. Introduction

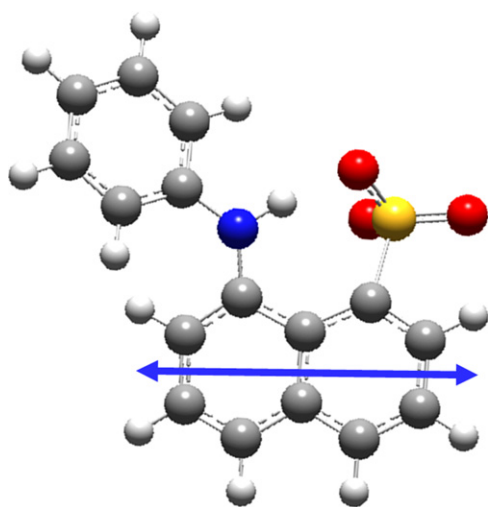
Ammonium 1-anilinoanthracene-8-sulfonate (ANS, Scheme 1), also known as a fluorescence dye, has been widely used as a probe *via* changing its fluorescence parameters (emission wavelength, quantum yield and lifetime), for the purpose of indicating the hydrophobic/hydrophilic circumstance [1,2], interactive locations [3,4] and the different conformation of proteins [5]. Owing to its sensitivity to environment, ANS was also applied to monitor the changes in pore volume of sol–gels [6]. In these cases, the luminescence of ANS is governed by its microenvironment, conformational changes and specific solute–solvent interactions. In addition, the peculiar fluorescence behavior of ANS in solid supramolecular environments, such as in solid complexes with α -, β -, γ -cyclodextrin and cyclophane CP 66, has been studied [7]. Wagner reported an interesting inclusion compound in which ANS molecules were co-crystallized in the lattice of a cucurbituril cages [8,9]. This structure is considered as a highly ordered solid solution and results in a strong fluorescence solid. Based on the previous

reports, it is known that both the immediate circumstance and the arrangement of ANS molecules are key factors influencing its fluorescence properties.

Layered double hydroxides (LDHs), whose structure can be generally expressed as $[M^{II}_{1-x}M^{III}_x(OH)_2](A^{n-})_{x/n} \cdot mH_2O$ (where M^{II} are divalent and M^{III} trivalent metals respectively, and A^{n-} an n -valent anion), are 2-D layered materials consisting of positively charged host layers with charge balancing guest anions. LDH materials have been extensively studied in the areas of catalysis [10,11], separation technology [12,13], drug delivery [14,15] and functional materials [16,17]. Synthesis of organic–inorganic hybrid materials based on LDHs has attracted much attention, for these materials may show special physicochemical characteristics which are not present in the individual components alone. Recently, the immobilization of photoactive molecules and their optic-functionalization with LDHs have been reported [18–21]. Our previous work [22] shows that the immobilization of guest molecules with a preferential arrangement in LDHs results in a desired alignment of photo-functional molecules in a macro-scale domain. This inspires us to challenge the goal of incorporation of ANS into LDH host matrix, which may possess the following advantages: (1) the solid matrix offers a confined environment for the immobilization and homogeneous distribution of dye molecules based on host–guest interactions, which can reduce dye aggregation and fluorescence quenching effectively; (2) the solid matrix would enhance the optical and thermal stability of the dye, which is a prerequisite to meet

* Corresponding author at: State Key Laboratory of Chemical Resource Engineering, Beijing University of Chemical Technology, Box 98, Science College, Beisanhuan East Road, Chaoyang Dis., Beijing 100029, China. Tel.: +86 10 64412131; fax: +86 10 64425385.

E-mail addresses: weimin@mail.buct.edu.cn, weimin-hewei@163.com (M. Wei).



Scheme 1. Molecular structure of ANS optimized by Gaussian 03 (C grey, H white, O red, N blue, S yellow). (For interpretation of the references to color in this scheme legend, the reader is referred to the web version of this article.)

the fabrication of solid state light emission device; (3) LDH materials exhibit the advantages of facile manipulation, low-cost and environment-friendliness. Although the fluorescence properties of ANS have been studied thoroughly in non-polar environments, its controllable luminescence behavior by using polar inorganic materials, especially immobilization into a layered host matrix is scarce and remains a challenge.

In this work, we report the incorporation of ANS into LDH matrix, and the composites are characterized by means of XRD, FT-IR, elemental analysis and TG/DTA thermal analysis. The luminescence properties of the composites can be tuned by changing the cation species and the molar ratio (M^{2+}/M^{3+}) of the LDH host layer. The influences of composition of LDH matrix on both the orientation and luminescence properties of interlayer chromophore have been studied and discussed thoroughly, for the purpose of obtaining superior photoluminescence materials based on host–guest interactions. Therefore, this work provides a new method for controlling the luminescence behavior of composite materials *via* regular arrangements of organic chromophores within an inorganic matrix, which can be potentially used in the field of photoluminescence.

2. Experimental

2.1. Materials

ANS was purchased from J&K Chemical Ltd. Analytical grade chemicals including $Zn(NO_3)_2 \cdot 6H_2O$, $Al(NO_3)_3 \cdot 9H_2O$, $Mg(NO_3)_2 \cdot 6H_2O$ and NaOH were purchased from the Beijing Chemical Co. Limited, and used without further purification. The deionized and decarbonate water was used in all the experimental processes.

2.2. Synthesis of ANS-LDH composites

The Zn_2Al-NO_3-LDH , Zn_3Al-NO_3-LDH , Mg_2Al-NO_3-LDH and Mg_3Al-NO_3-LDH precursors were synthesized by the hydrothermal method reported previously [23]. A solution of $NH_3 \cdot H_2O$ (25%) was added dropwise to a solution (200 mL) containing $Zn(NO_3)_2 \cdot 6H_2O$ and $Al(NO_3)_3 \cdot 9H_2O$ (molar ratio 2:1) with vigorous stirring under nitrogen. The pH value of the solution at the end of addition was 8.5. The suspension was transferred to an autoclave and heated at $140^\circ C$ for 10 h. The resulting precipitate was separated by centrifugation, washed thoroughly with deionized water.

Subsequently, the ANS intercalated LDHs were prepared by the ion-exchange method as following: ANS (1.2 g) was dissolved in a mixture solution of ethanol–water (1:1, v/v) with pH adjusted to 7.5 by adding NaOH solution (0.1 M), and then 1.50 g of freshly prepared Zn_2Al-NO_3-LDH (0.51 g, 1.62 mmol after drying) was added. The mixture was stirred at $70^\circ C$ under N_2 atmosphere for 48 h. The resulting precipitate $Zn_2Al-ANS-LDH$ was centrifuged, washed thoroughly with ethanol and water. $Zn_3Al-ANS-LDH$, $Mg_2Al-ANS-LDH$ and $Mg_3Al-ANS-LDH$ were synthesized according to a similar procedure. Elemental analysis: found ($Zn_2Al-ANS-LDH$) Zn 23.18%, Al 6.86%, C 23.01%, N 2.98%, S 3.48%, H 3.52%; found ($Zn_3Al-ANS-LDH$) Zn 40.07%, Al 6.20%, C 28.91%, N 3.71%, S 4.72%, H 4.47%; found ($Mg_2Al-ANS-LDH$) Mg 10.71%, Al 6.14%, C 39.74%, N 3.41%, S 6.27%, H 5.26%; found ($Mg_3Al-ANS-LDH$) Mg 10.32%, Al 4.97%, C 29.41%, N 2.63%, S 4.44%, H 4.11%.

2.3. Fabrication of ANS-LDH Thin Films

Thin film of $Zn_2Al-ANS-LDH$ was fabricated by the solvent evaporation method. Substrates of Si wafer were firstly cleaned by immersing in a bath of H_2SO_4/H_2O_2 (3/1, v/v) and then were treated in an ultrasonic bath for 30 min. Pasty $Zn_2Al-ANS-LDH$ (0.05 g) was suspended in water (25 mL) in a glass flask and treated in an ultrasonic bath under N_2 atmosphere for 5 min. The resulting $Zn_2Al-ANS-LDH$ suspension was dropped on Si substrates and dried in vacuum at ambient temperature for 5 h. The thin films of $Zn_3Al-ANS-LDH$, $Mg_2Al-ANS-LDH$ and $Mg_3Al-ANS-LDH$ were fabricated following the same procedure.

2.4. Techniques of characterization

The powder XRD measurements were performed on a Rigaku XRD-6000 diffractometer, using $Cu K\alpha$ radiation ($\lambda = 0.15418$ nm) at 40 kV, 30 mA, with a scanning rate of $10^\circ/\text{min}$, and a 2θ angle ranging from 3° to 70° . FT-IR spectra were recorded on a Bruker Vector 22 Fourier transfer infrared spectrophotometer using the KBr disk method in the range from 4000 to 400 cm^{-1} , with a resolution of 2 cm^{-1} and accumulation of 32 scans. SEM images were obtained using a Hitachi S-4700 scanning electron microscope operating at 20 kV. Metallic elemental analysis was performed by atomic emission spectroscopy with a Shimadzu ICPS-7500 instrument. C, H, N content was determined using an Elementar vario elemental analysis instrument. Thermogravimetry and differential thermal analysis (TG–DTA) curves were obtained on a Beifen PCT-1A instrument in the temperature range $25\text{--}700^\circ C$. The solid UV–vis adsorption spectra were collected in the range from 200 to 600 nm on a Pukinje General TU-1901 with the slit width of 1.0 nm, and $BaSO_4$ was used as reference. The fluorescence spectra were performed on RF-5301PC fluorospectrophotometer under the identical condition with excitation wavelength of 370 nm and emission spectra in the range 400–600 nm.

2.5. Fluorescence polarization

The fluorescence polarization technology was used to determine the orientation of ANS, and was performed according to the method reported by our group previously with some modifications [22]. Thin films of ANS-LDHs were fabricated according to the same procedure as reported by our group [22]. The spectra of the composites film were registered after excitation at 370 nm and scanned in the range 425–600 nm. The angle between the normal to the thin film and the excitation axis (defined as the δ angle) was scanned from 40° to 70° . To correct the instrumental response to the linearly polarized light, 1.5×10^{-5} mol/L and 4.0×10^{-5} mol/L of ANS ethanol solutions were used as the isotropic system for $ZnAl-ANS-LDH$ and $MgAl-ANS-LDH$ system, respectively.

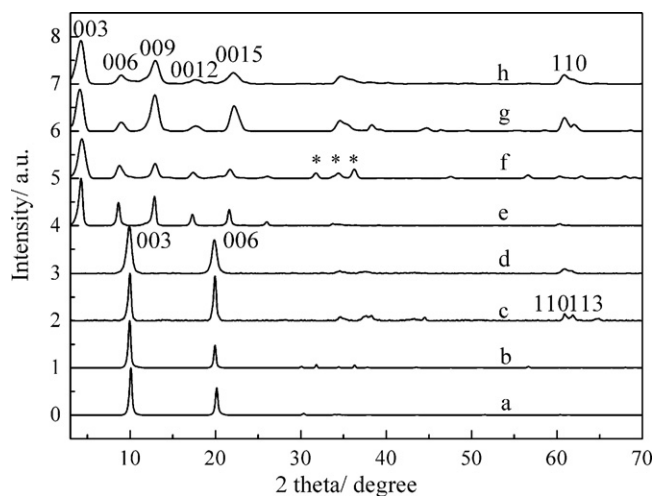


Fig. 1. Powder XRD patterns for (a) $\text{Zn}_2\text{Al-NO}_3\text{-LDH}$, (b) $\text{Zn}_3\text{Al-NO}_3\text{-LDH}$, (c) $\text{Mg}_2\text{Al-NO}_3\text{-LDH}$, (d) $\text{Mg}_3\text{Al-NO}_3\text{-LDH}$, (e) $\text{Zn}_2\text{Al-ANS-LDH}$, (f) $\text{Zn}_3\text{Al-ANS-LDH}$, (g) $\text{Mg}_2\text{Al-ANS-LDH}$ and (h) $\text{Mg}_3\text{Al-ANS-LDH}$. Asterisk denotes the reflections of ZnO impurity.

As quantum mechanic calculations suggested, 1-substituted naphthalenes exhibit mainly *a*-type activity, i.e., the $S_0 \rightarrow S_1$ transitions of 1-substituted naphthalenes is polarized along the long in-plane axis [24]. Therefore, the transitional direction of ANS molecule is along its long axis [25,26] (as shown in Scheme 1).

The responses of fluorescence spectrum of the ANS film to horizontally (H) and vertically (V) polarized incident light were recorded by varying the orientation angle δ between the normal to the film and the incident light. A linear relationship between the fluorescence dichroic ratio (D_{HV} was defined as the ratio of H and V polarized emission spectra, $D_{\text{HV}} \equiv I_{\text{HH}}/I_{\text{HV}}$) and the twist angle δ (with a right-angle configuration between the excitation and the emission beam) was established by means of:

$$(D_{\text{HV}})^{\text{cor}} = \frac{I_{\text{HV}}}{I_{\text{VH}}} \times G = 2 \cot^2 \psi + (1 - 2 \cot^2 \psi) \cos^2(90 + \delta)$$

where G is the instrumental G factor which makes a correction for the instrumental response to the emission H and V polarizer by taking into account the evolution of the fluorescence band of an isotropic system with the twist angles δ recorded under identical conditions, i.e., ($G \equiv (I_{\text{HV}}/I_{\text{HH}})^{\text{iso}}$). An aqueous solution of ANS was used as the isotropic system. From the corresponding slope and/or intercept of a plot of $(D_{\text{HV}})^{\text{cor}}$ vs. $\cos^2(90 + \delta)$, the relative orientation of the interlayer ANS can be evaluated in terms of the angle ψ (defined as the angle between the transition moment of ANS and the normal to the LDH layer) (Figs. S1 and S2).

3. Results and discussion

3.1. Characterization of the ANS-LDH composites

The powder XRD patterns of LDH precursors, $\text{Zn}_2\text{Al-ANS-LDH}$, $\text{Zn}_3\text{Al-ANS-LDH}$, $\text{Mg}_2\text{Al-ANS-LDH}$ and $\text{Mg}_3\text{Al-ANS-LDH}$ are shown in Fig. 1, respectively. In each case, the reflections can be indexed to a hexagonal lattice with $R\bar{3}m$ rhombohedral symmetry, commonly used for the description of the LDH structures. For the four LDH precursors (Fig. 1a–d), the 003 reflection gives the interlayer distance of 8.92, 8.91, 8.89 and 8.94 Å respectively, in accordance with the reported value for $\text{NO}_3\text{-LDH}$ [27]. After the anion-exchange reaction, the basal reflection (003) of ANS-LDH composites (Fig. 1e–h) shifted to lower 2θ angles, and the basal spacing expanded to 19.6, 20.1, 21.5 and 21.6 Å for the $\text{Zn}_2\text{Al-ANS-LDH}$, $\text{Zn}_3\text{Al-ANS-LDH}$, $\text{Mg}_2\text{Al-ANS-LDH}$ and $\text{Mg}_3\text{Al-ANS-LDH}$ samples, respectively. The results indicate that ANS anions have been intercalated into the

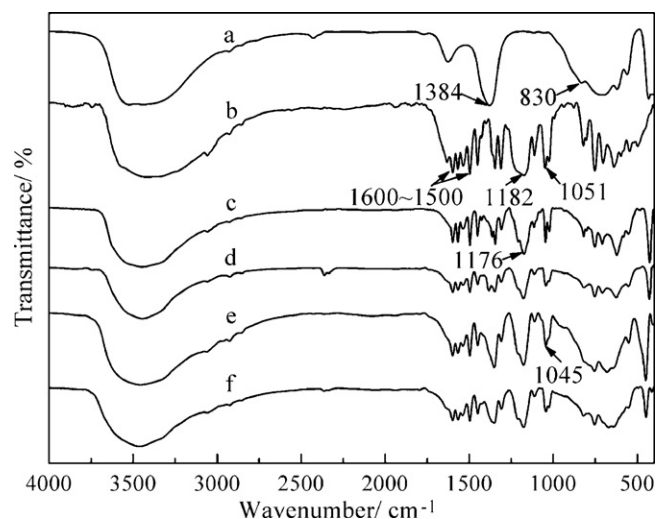


Fig. 2. FT-IR spectra of (a) $\text{NO}_3\text{-LDH}$, (b) ANS, (c) $\text{Zn}_2\text{Al-ANS-LDH}$, (d) $\text{Zn}_3\text{Al-ANS-LDH}$, (e) $\text{Mg}_2\text{Al-ANS-LDH}$ and (f) $\text{Mg}_3\text{Al-ANS-LDH}$.

LDH lamellar. The compositions of the LDH precursors and resulting products are listed in Table 1, and the XRD parameters (d_{003} and a) are also presented. It can be seen that a little amount of NO_3^- co-existed with ANS anions in LDH galleries.

The FT-IR spectra of $\text{NO}_3\text{-LDH}$, ANS, $\text{Zn}_2\text{Al-ANS-LDH}$, $\text{Zn}_3\text{Al-ANS-LDH}$, $\text{Mg}_2\text{Al-ANS-LDH}$ and $\text{Mg}_3\text{Al-ANS-LDH}$ are shown in Fig. 2, respectively. For the sake of clarity, only the main absorption bands were listed. The spectrum of $\text{NO}_3\text{-LDH}$ (Fig. 2a) shows a strong absorption band at 1384 cm^{-1} and a weak one at 830 cm^{-1} that can be attributed to the ν_3 and ν_2 stretching vibration of NO_3^- group respectively. The characteristic absorption band of carbonate at 1360 cm^{-1} was not observed, confirming the absence of carbonate in precursors. In the spectrum of pristine ANS (Fig. 2b), the strong absorption bands at 1182 and 1051 cm^{-1} are due to the O=S=O stretching vibration of the sulfonate group [28,29]. The absorption bands in the region $1500\text{--}1600 \text{ cm}^{-1}$ are attributed to the benzene vibration. The four spectra of ANS-LDH composites (Fig. 2c–f) display characteristic bands of $-\text{SO}_3^-$ group at 1176 and 1045 cm^{-1} with a red-shift of $6\text{--}8 \text{ cm}^{-1}$ compared with pristine ANS, as a result of host–guest interactions between LDH matrix and ANS [30]. Compared with the $\text{NO}_3\text{-LDH}$ precursor (Fig. 2a), the intensity of absorption band attributed to NO_3^- at 1384 cm^{-1} decreases significantly for the ANS-LDH composites, confirming that the ANS anion and NO_3^- coexist in the galleries of LDH. This is in agreement with the elemental analysis results (Table 1).

The morphology of composites (both the powder and thin film) revealed by SEM is shown in Fig. 3. The powder samples (Fig. 3a–d) afford a rough surface composed of randomly oriented LDH particles with irregular morphology. In contrast, the thin films of ANS-LDH (Fig. 3e–h) exhibit a smooth and continuous surface in the top view and also demonstrate that the individual ANS-LDH platelets are densely packed on the substrate with well *c* orientation. A few claviform crystalloids which could be attributed to a ZnO impurity phase were observed for the $\text{Zn}_3\text{Al-ANS-LDH}$ sample (Fig. 3f), consistent with the XRD results.

3.2. Orientation of ANS intercalated in LDH determined by the fluorescent polarization

The preferential orientation of ANS intercalated into LDHs was obtained by the fluorescence polarization technology. The results show that the values of orientation angle (ψ) were calculated to be 58° for $\text{Zn}_2\text{Al-ANS-LDH}$, 57° for $\text{Zn}_3\text{Al-ANS-LDH}$, 55° for $\text{Mg}_2\text{Al-ANS-LDH}$ and 52° for $\text{Mg}_3\text{Al-ANS-LDH}$ respectively (see Section

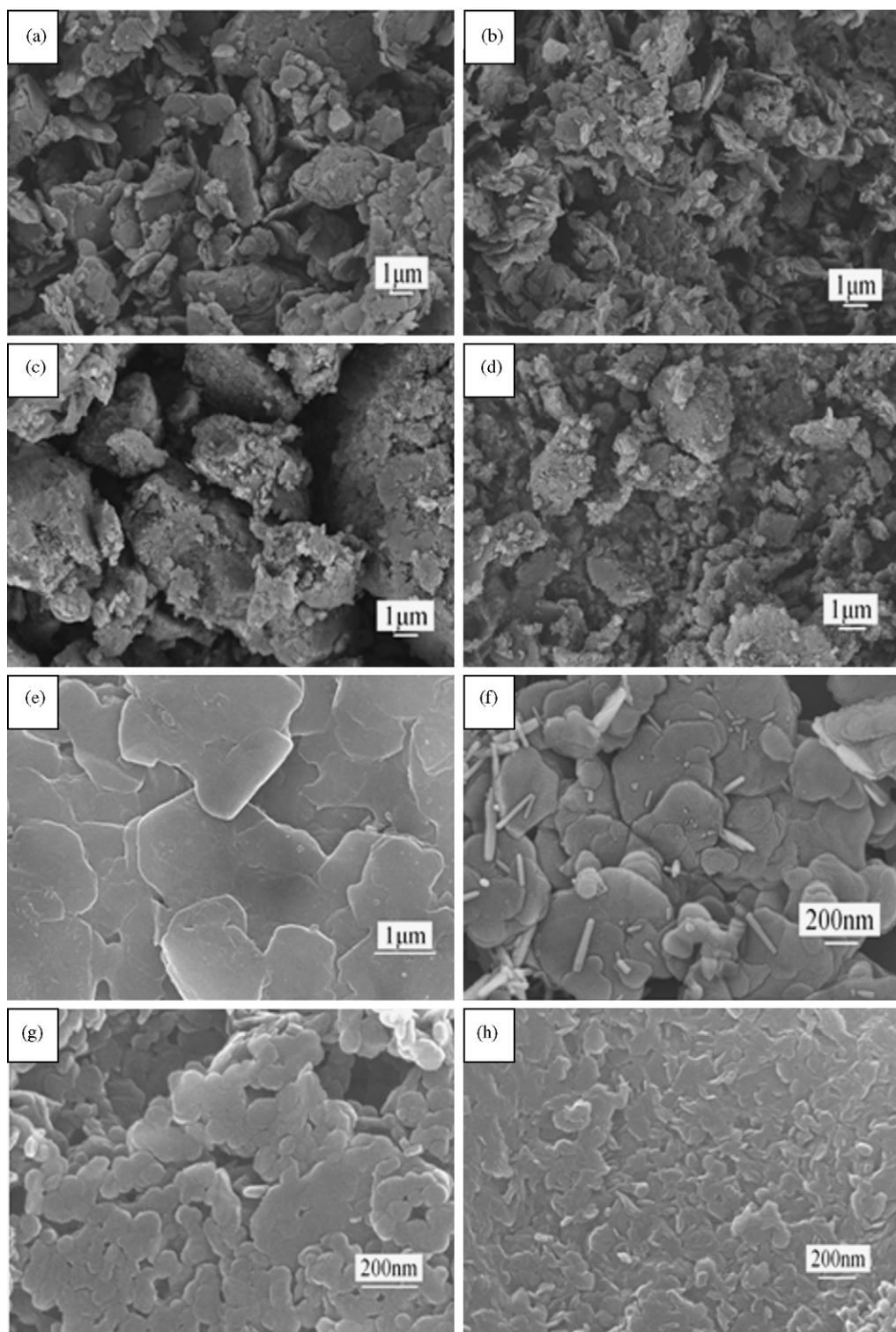


Fig. 3. SEM images of the powder samples of (a) Zn₂Al-ANS-LDH, (b) Zn₃Al-ANS-LDH, (c) Mg₂Al-ANS-LDH, (d) Mg₃Al-ANS-LDH and the thin film samples of (e) Zn₂Al-ANS-LDH, (f) Zn₃Al-ANS-LDH, (g) Mg₂Al-ANS-LDH, (h) Mg₃Al-ANS-LDH.

2: 370 nm of excitation). The orientation of ANS for the samples of Zn₂Al-ANS-LDH and Mg₂Al-ANS-LDH was also determined by measuring the linearly polarized spectra at 390 nm (Fig. S3), and the values obtained are in agreement to that of at 370 nm. The $(D_{HV})^{cor}$ value is practically independent of the emission wavelength, indicating the presence of only one type of ANS species for an individual sample. According to the report of Arbeloa et al. on the polarization technology, the difference of 1° in orien-

tation angle is significant and accounts for the varieties in system [31,32].

Furthermore, based on the basal spacing d_{003} of the composites obtained from XRD, the values of gallery height were calculated to be 1.48, 1.53, 1.67 and 1.68 nm for Zn₂Al-ANS-LDH, Zn₃Al-ANS-LDH, Mg₂Al-ANS-LDH and Mg₃Al-ANS-LDH respectively, by subtracting the thickness of the inorganic layer (0.48 nm). Taking into account the molecular dimensions of ANS (0.68 nm for ANS

Table 1
Chemical compositions and unit-cell parameters for NO₃-LDHs and ANS-LDHs.

M ²⁺ /M ³⁺ initial ratio	Chemical composition	d ₀₀₃ (Å)	a (Å)
2:1	Zn _{0.632} Al _{0.368} (OH) ₂ (NO ₃) _{0.368} ·0.45H ₂ O	8.92	3.03
2:1	Zn _{0.637} Al _{0.363} (OH) ₂ (ANS) _{0.211} (NO ₃) _{0.152} ·0.97H ₂ O	19.6	3.06
3:1	Zn _{0.732} Al _{0.268} (OH) ₂ (NO ₃) _{0.268} ·0.58H ₂ O ^a	8.91	3.04
3:1	Zn _{0.726} Al _{0.274} (OH) ₂ (ANS) _{0.165} (NO ₃) _{0.109} ·0.75H ₂ O ^a	20.1	3.06
2:1	Mg _{0.647} Al _{0.353} (OH) ₂ (NO ₃) _{0.353} ·0.56H ₂ O	8.89	3.04
2:1	Mg _{0.646} Al _{0.354} (OH) ₂ (ANS) _{0.286} (NO ₃) _{0.044} (CO ₃) _{0.012} ·1.33H ₂ O	21.5	3.04
3:1	Mg _{0.718} Al _{0.282} (OH) ₂ (NO ₃) _{0.282} ·0.47H ₂ O	8.94	3.04
3:1	Mg _{0.715} Al _{0.285} (OH) ₂ (ANS) _{0.223} (NO ₃) _{0.042} (CO ₃) _{0.010} ·1.07H ₂ O	21.6	3.04

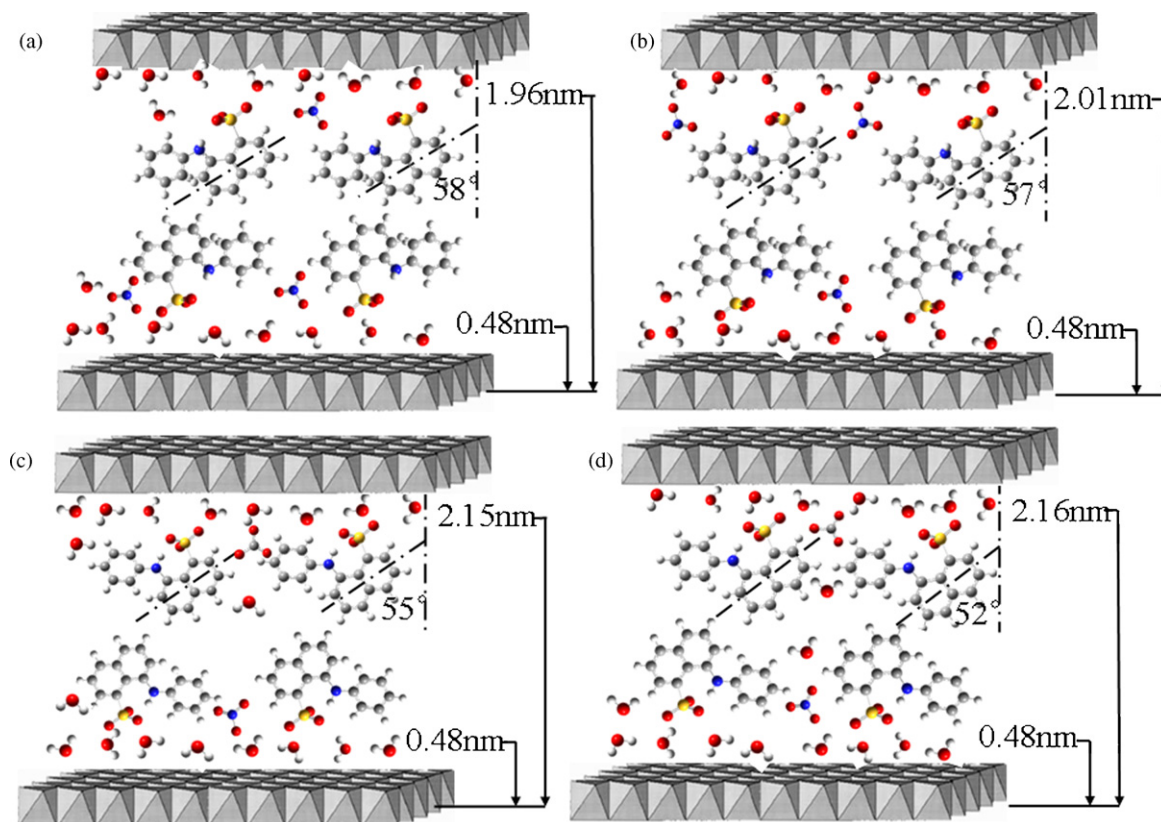
^a Owing to the low content of ZnO impurity, the two Zn₃Al-LDH samples were approximately represented as a pure LDH composition.

calculated by Gaussian 03), it can be speculated that ANS is accommodated in the interlayer region as double layer. On the basis of ANS dimension and its orientation, the schematic structures of ANS-LDH composites were tentatively proposed and presented in Scheme 2.

3.3. Thermal stability of the ANS-LDH composites

The four composites show very similar thermal decomposition behavior, as a result the Zn₂Al-ANS-LDH sample was taken as an example. TG-DTA curves of the pristine ANS, Zn₂Al-NO₃-LDH and Zn₂Al-ANS-LDH are displayed in Fig. 4, respectively. A weight loss around 70–130 °C was observed for the pure ANS (Fig. 4A), due to the loss of crystalline water. Subsequently a rapid weight loss in the temperature range 325–580 °C occurred accompanied with exothermic peaks in the DTA curve, corresponding to the combustion of the organic molecule. For the thermal decomposition of Zn₂Al-NO₃-LDH (Fig. 4B), the weight loss below 125 °C with an endothermic peak in the DTA curve corresponds to the loss of crystalline water [33]. Upon increasing temperature, two weight

loss stages in 180–290 and 290–500 °C were observed, which can be attributed to the dehydroxylation and decomposition of nitrate ions [34]. In the case of Zn₂Al-ANS-LDH sample (Fig. 4C), several endothermic peaks noted at 70–180 °C in the DTA curve correspond to the removal of surface adsorbed and interlayer water molecules [33,34]. A rapid and major mass loss due to the dehydroxylation and decomposition of interlayer ANS anions in 180–560 °C occurs, and the first exothermic peak related to the decomposition of ANS anions shifts from 325 (Fig. 4A) to 360 °C (Fig. 4C). A similar phenomenon was also observed in the case of Zn₃Al-ANS-LDH, Mg₂Al-ANS-LDH and Mg₃Al-ANS-LDH. Consequently, it can be concluded that the thermal stability of ANS was enhanced to some extent after intercalation into LDH matrix owing to the presence of host-guest interactions. The thermal stability of ANS in LDH matrix was further studied by recording the correlation between fluorescence intensity and heat treatment for the ANS-LDH composites. Fig. S4 shows the variation of fluorescence intensity for the three samples (Zn₂Al-ANS-LDH, Mg₂Al-ANS-LDH and pristine ANS) along with heat treatment temperature, from which a much slower decrease in fluorescence intensity of Zn₂Al-ANS-LDH and Mg₂Al-



Scheme 2. A possible representation for the structures of (a) Zn₂Al-ANS-LDH, (b) Zn₃Al-ANS-LDH, (c) Mg₂Al-ANS-LDH and (d) Mg₃Al-ANS-LDH (C grey, H white, O red, N blue, S yellow). (For interpretation of the references to color in this scheme legend, the reader is referred to the web version of this article.)

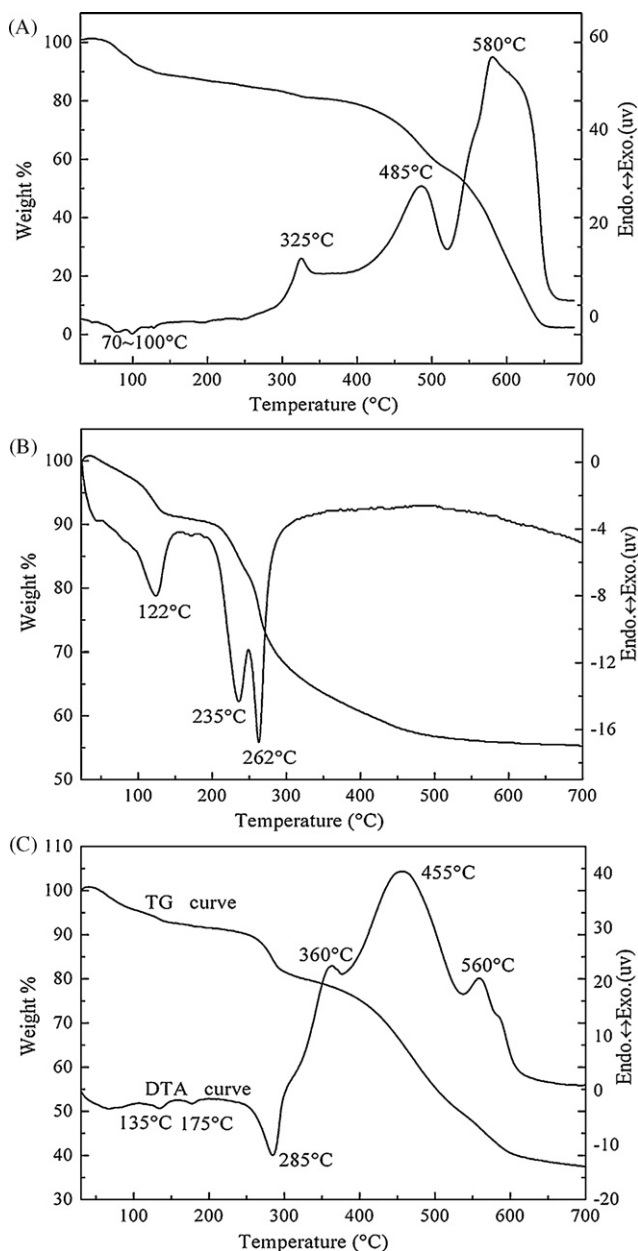


Fig. 4. TG-DTA curves for (A) ANS, (B) Zn_2Al-NO_3-LDH and (C) $Zn_2Al-ANS-LDH$.

ANS-LDH was observed compared with pristine ANS. This indicates that the thermal stability of ANS was enhanced upon intercalation into LDH matrix, in agreement with the result of TG-DTA.

3.4. UV-vis absorption and fluorescence spectroscopy

The UV-vis absorption spectra of the composites are shown in Fig. 5, with comparison samples of ANS in ethanol solution, solid ANS and physical mixture of ANS with Zn_3Al-NO_3-LDH , and the maximum absorption wavelength are listed in Table 2. Compared with ANS in solution (curve g, 370 nm), a red-shift of ~ 36 nm was observed for the solid ANS sample, which can be attributed to the J-type aggregate of ANS. A blue-shift of ~ 6 nm was observed for the physical mixture compared with pristine ANS, which can be attributed to the decrease in aggregation of ANS by adding Zn_3Al-NO_3-LDH [7]. For the ANS-LDH composites, the λ_{max} of ANS ranges in 385–400 nm (curve a–d in Fig. 5), larger than ANS in ethanol solution (370 nm) but less than solid ANS (406 nm). This

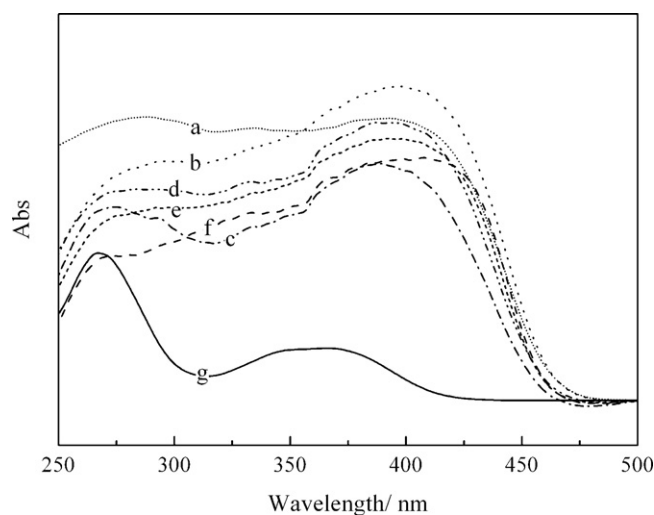


Fig. 5. UV-vis absorption spectra of (a) $Zn_2Al-ANS-LDH$, (b) $Zn_3Al-ANS-LDH$, (c) $Mg_2Al-ANS-LDH$, (d) $Mg_3Al-ANS-LDH$, (e) physical mixture of ANS with Zn_3Al-NO_3-LDH , (f) pristine ANS and (g) ANS in ethanol solution (10^{-4} mol/L).

Table 2

The maximum wavelength of absorption and emission of the ANS-LDH composites.

	λ_{max} (nm)	λ_{em} (nm)
$Zn_2Al-ANS-LDH$	398	487
$Zn_3Al-ANS-LDH$	400	490
$Mg_2Al-ANS-LDH$	385	496
$Mg_3Al-ANS-LDH$	385	499
Pristine ANS	406	484
Physical mixture of ANS and Zn_3Al-NO_3-LDH	400	482
ANS in ethanol solution (10^{-4} mol/L)	370	470

indicates that the J-type aggregate of ANS may exist in the galleries of LDH [35].

In ANS ethanol solution, a gradual red-shift for the maximum emission band from 470 to 481 nm as well as fluorescence quenching were observed upon increasing the dye concentration in the range 1.0×10^{-5} – 5.0×10^{-3} mol/L, indicating the formation of J-type aggregate of ANS (Fig S5) [36–38]. Fig. 6 displays the fluorescence spectra of the ANS-LDH composites, which are significantly different from that of pristine ANS. The fluorescence intensity obeys

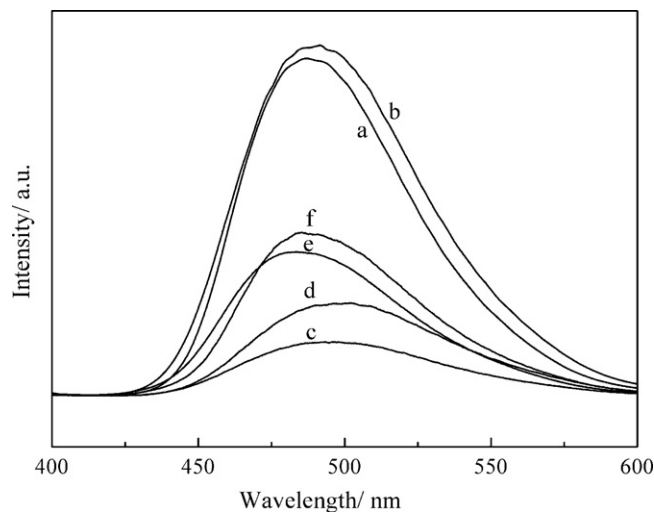


Fig. 6. Fluorescence spectra of the composites of (a) $Zn_2Al-ANS-LDH$, (b) $Zn_3Al-ANS-LDH$, (c) $Mg_2Al-ANS-LDH$, (d) $Mg_3Al-ANS-LDH$, (e) the mixture of ANS and Zn_3Al-NO_3-LDH , (f) pristine ANS. λ_{ex} = 370 nm.

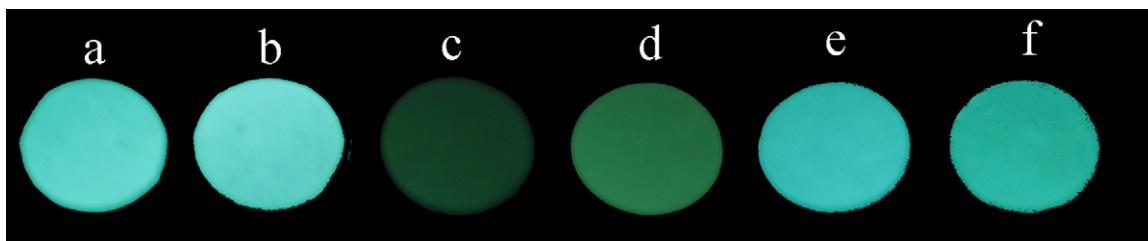


Fig. 7. Photographs of (a) Zn₂Al-ANS-LDH, (b) Zn₃Al-ANS-LDH, (c) Mg₂Al-ANS-LDH, (d) Mg₃Al-ANS-LDH, (e) mixture of ANS and Zn₃Al-NO₃-LDH and (f) pristine ANS under UV irradiation of 365 nm.

the following order: Zn₃Al-ANS-LDH > Zn₂Al-ANS-LDH > Mg₃Al-ANS-LDH > Mg₂Al-ANS-LDH. For the two ZnAl-ANS-LDH samples (curve a and b in Fig. 6), they exhibit strong fluorescence intensity, which is about three times higher than that of pristine ANS solid sample (curve f). However, ANS intercalated into MgAl-LDH samples (curve c and d in Fig. 6) emit relative weaker fluorescence compared with that of pristine ANS. For the physical mixture of Zn₃Al-NO₃-LDH and ANS, a blue-shift was found for the emission spectra compared with pristine ANS, indicating that the aggregation was reduced by the dilution effect of Zn₃Al-NO₃-LDH. The changes in fluorescence of these samples are further demonstrated by their photographs with irradiation by UV light (365 nm), from which ZnAl-ANS-LDHs show much stronger brightness in blue than that of MgAl-ANS-LDHs (Fig. 7). The enhancement of fluorescence intensity of ANS in the ZnAl-LDH matrix can be attributed to its low aggregation degree in LDH gallery. It can be seen from the chemical composition (Table 1) that the molar concentration of ANS in ZnAl-LDHs is much lower than that of MgAl-LDHs. Consequently, the lower content of ANS in the ZnAl-LDH matrix leads to lower aggregation and thus stronger intensity of fluorescence emission.

It is also worth noticing that the fluorescence intensity of ANS-LDH composites increases with the molar ratio M²⁺/Al³⁺ of LDH from 2:1 to 3:1, which was further observed in their photographs with UV light irradiation (shown in Fig. 7). This can be attributed to the decrease in aggregation of ANS upon increasing the M²⁺/Al³⁺ in LDH matrix. It is known that the anion in the interlayer galleries combines with LDH-sheet by electrostatic force. Therefore, the concentration of interlayer ANS can be controlled by the charge density of host layers, i.e., the M²⁺/Al³⁺ ratio. Higher M²⁺/Al³⁺ ratio leads to lower charge density and thus lower concentration of interlayer ANS. Owing to the previous report that M²⁺ and M³⁺ are ordered distributed and no Al³⁺-Al³⁺ contacts exist in the LDH hydroxide layers [39], the average distance of Al³⁺-Al³⁺ in the LDH with M²⁺/Al³⁺ of 3:1 is larger than that of 2:1, which results in the well-proportioned distribution and the decrease in aggregation of ANS molecules in the LDH gallery. This is also in accordance with the results of elemental analysis (Table 1) that a higher content of ANS was observed in the composites with M²⁺/Al³⁺ of 2:1 than that of 3:1. The results above indicate that both the host-guest interaction (controlled by the metal type in LDH layers) and the guest-guest interaction (tuned by the M²⁺/Al³⁺ ratio) are key factors in determining the fluorescence properties of ANS in LDH matrix.

4. Conclusions

The ANS molecule has been incorporated into the ZnAl-NO₃-LDH and MgAl-NO₃-LDH matrix by ion-exchange method, respectively. XRD and FT-IR indicate the successful intercalation of ANS into galleries of LDHs. TG-DTA shows that the thermal stabilities of intercalated ANS exhibit a notable increase compared with that of pristine ANS. The fluorescence polarization was employed to evaluate the preferential orientation of the interlayer ANS molecules, and the structures of ANS-LDHs composites were proposed. The

fluorescence intensity follows the orders: Zn₃Al-ANS-LDH > Zn₂Al-ANS-LDH > Mg₃Al-ANS-LDH > Mg₂Al-ANS-LDH, which was further demonstrated by the photograph of the samples with UV light irradiation. It was found that both the metal type in LDH layers and the M²⁺/Al³⁺ ratio show significant influences on the fluorescence properties of ANS in LDH matrix. Therefore, it can be concluded that the luminescence of ANS molecules is dependent upon the confinement effect imposed by LDH matrix, and can be simply tuned by changing the two factors mentioned above. This work provides a facile method for the immobilization and dispersion of organic dyes within a 2D inorganic matrix, for the purpose of prospective application in solid photoluminescence materials.

Acknowledgements

This project was supported by the National Natural Science Foundation of China, the 111 Project (Grant No. B07004), the 973 Program (Grant No. 2009CB939802) and the Fundamental Research Funds for the Central Universities (Grant No. ZZ0908).

Appendix A. Supplementary data

Supplementary data associated with this article can be found, in the online version, at doi:10.1016/j.cej.2010.04.031.

References

- [1] D. Rajalingam, I. Graziani, I. Prudovsky, C. Yu, T.K.S. Kumar, Relevance of partially structured states in the non-classical secretion of acidic fibroblast growth factor, *Biochemistry* 46 (2007) 9225–9238.
- [2] Z.W. Ma, G. Piszczek, P.T. Wingfield, Y.V. Sergeev, J.F. Hejtmanick, The G18V CRYGS mutation associated with human cataracts increases γ S-crystallin sensitivity to thermal and chemical stress, *Biochemistry* 48 (2009) 7334–7341.
- [3] R. Tagore, H.R. Thomas, E.A. Homan, A. Munawar, A. Saghatelian, A global metabolite profiling approach to identify protein-metabolite interactions, *J. Am. Chem. Soc.* 130 (2008) 14111–14113.
- [4] T. Ohashi, A.M. Augustus, H.P. Erickson, Transient opening of fibronectin type III (FN^{III}) domains: the interaction of the third FN^{III} domain of FN with anastellin, *Biochemistry* 48 (2009) 4189–4197.
- [5] A.M. Tan, M.T. Henzl, Evidence for a Ca²⁺-specific conformational change in avian thymic hormone, a high-affinity β -parvalbumin, *Biochemistry* 48 (2009) 3936–3945.
- [6] M.C. Burt, B.C. Dave, Externally tunable dynamic confinement effect in organosilica sol-gels, *J. Am. Chem. Soc.* 128 (2006) 11750–11751.
- [7] H.J. Buschmann, T. Wolff, Fluorescence of 1-anilinonaphthalene-8-sulfonate in solid macrocyclic environments, *J. Photochem. Photobiol. A: Chem.* 121 (1999) 99–103.
- [8] B.D. Wagner, A.I. MacRae, The lattice inclusion compound of 1,8-ANS and cucurbituril: a unique fluorescent solid, *J. Phys. Chem. B* 103 (1999) 10114–10119.
- [9] B.D. Wagner, N. Stojanovic, A.I. Day, R.J. Blanch, Host properties of cucurbit[7]uril: fluorescence enhancement of anilinonaphthalene sulfonates, *J. Phys. Chem. B* 107 (2003) 10741–10746.
- [10] V.R.L. Constantino, T.J. Pinnavaia, Structure-reactivity relationships for basic catalysts derived from a Mg²⁺/Al³⁺/CO₃²⁻ layered double hydroxide, *Catal. Lett.* 23 (1994) 361–367.
- [11] A. Corma, V. Fornes, F. Rey, A. Cervilla, E. Llopis, A. Ribera, Catalytic air oxidation of thiols mediated at a Mo(VI)O₂ complex center intercalated in a Zn(II)-Al(III) layered double hydroxide host, *J. Catal.* 152 (1995) 237–242.
- [12] T. Kameda, T. Yamazaki, T. Yoshioka, Selective uptake of aromatic compounds from aqueous solutions by Mg–Al layered double hydroxide intercalated with 2,7-naphthalenedisulfonate, *Chem. Lett.* 38 (2009) 522–523.

- [13] T. Kameda, M. Saito, Y. Umetsu, Uptake of bisphenol A from aqueous solution by Mg–Al-layered double hydroxides intercalated with 2-Naphthalene sulfonate and 2,6-naphthalene disulfonate, *Mater. Trans.* 48 (2007) 2225–2229.
- [14] A.I. Khan, A.J. Norquist, D. O'Hare, Intercalation and controlled release of pharmaceutically active compounds from a layered double hydroxide, *Chem. Commun.* 22 (2001) 2342–2343.
- [15] J.H. Choy, J.S. Jung, J.M. Oh, M. Park, J. Jeong, Y.K. Kang, O.J. Han, Layered double hydroxide as an efficient drug reservoir for folate derivatives, *Biomaterials* 25 (2004) 3059–3064.
- [16] T. Kameda, Y. Tsuchiya, T. Yamazaki, T. Yoshioka, Preparation of Mg–Al layered double hydroxides intercalated with alkyl sulfates and investigation of their capacity to take up N,N-dimethylaniline from aqueous solutions, *Solid State Sci.* 11 (2009) 2060–2064.
- [17] T. Yoshioka, W. Kouji, U. Miho, A. Okuwaki, Dehydrochlorination behavior of a chloride ion-intercalated hydrotalcite-like compound during thermal decomposition, *Mater. Trans.* 47 (2006) 923–930.
- [18] J. Bauer, P. Behrens, M. Speckbacher, H. Langhals, Composites of perylene chromophores and layered double hydroxides: direct synthesis, characterization, and photo- and chemical stability, *Adv. Funct. Mater.* 13 (2003) 241–248.
- [19] K. Lang, P. Bezdička, J.L. Bourdelande, J. Hernando, I. Jirka, E. Káfuňková, F. Kovanda, P. Kubát, J. Mosinger, D.M. Wagnerová, Layered double hydroxides with intercalated porphyrins as photofunctional materials: subtle structural changes modify singlet oxygen production, *Chem. Mater.* 19 (2007) 3822–3829.
- [20] T. Saito, J.I. Kadokawa, H. Tagaya, Repartition of organic–inorganic layered nanohybrids by intercalation of photofunctional compounds, *Trans. Mater. Res. Soc. Jpn.* 26 (2001) 503–506.
- [21] S.H. Hwang, Y.S. Han, J.H. Choy, Intercalation of functional organic molecules with pharmaceutical, cosmeceutical and nutraceutical functions into layered double hydroxides and zinc basic salts, *Bull. Korean Chem. Soc.* 22 (2001) 1019–1022.
- [22] W.Y. Shi, M. Wei, J. Lu, F. Li, J. He, D.G. Evans, X. Duan, Molecular orientation and fluorescence studies on naphthalene acetate intercalated Zn₂Al layered double hydroxide, *J. Phys. Chem. C* 112 (2008) 19886–19895.
- [23] R.P. Bontchev, S. Liu, J.L. Krumhansl, J. Voigt, T.M. Nenoff, Synthesis, characterization, and ion exchange properties of hydrotalcite Mg₆Al₂(OH)₁₆(A)_x(A')_{2–x}·4H₂O (A, A' = Cl[–], Br[–], I[–], and NO₃[–], 2 ≥ x ≥ 0) derivatives, *Chem. Mater.* 15 (2003) 3669–3675.
- [24] G. Berden, L. Meerts, D. Plusquellic, I. Fujita, D. Pratt, High resolution electronic spectroscopy of 1-aminonaphthalene: S₀ and S₁ geometries and S₁ ← S₀ transition moment orientations, *J. Chem. Phys.* 104 (1996) 3935–3946.
- [25] E. Klimtchuk, S. Venyaminov, E. Kurian, W. Wessels, W. Kirk, F.G. Prendergast, Photophysics of ANS. I. Protein–ANS complexes: intestinal fatty acid binding protein and single-*trp* mutants, *Biophys. Chem.* 125 (2007) 1–12.
- [26] W. Kirk, Photophysics of ANS. II. Charge transfer character of near-UV absorption and consequences for ANS spectroscopy, *Biophys. Chem.* 125 (2007) 13–23.
- [27] A. Legroui, M. Badreddine, A. Barrou, A. DeRoy, J.P. Besse, Influence of pH on the synthesis of the Zn–Al-nitrate layered double hydroxide and the exchange of nitrate by phosphate ions, *J. Mater. Sci. Lett.* 18 (1999) 1077–1079.
- [28] F. Camerel, J. Barberá, J. Otsuki, T. Tokimoto, Y. Shimazaki, L.Y. Chen, S.H. Liu, M.S. Lin, C.C. Wu, R. Ziesel, Solution-processable liquid crystals of luminescent aluminum(8-hydroxyquinoline-5-sulfonato) complexes, *Adv. Mater.* 20 (2008) 3462–3467.
- [29] R. Marangoni, M. Bouhent, C. Taviot-Guého, F. Wypych, F. Leroux, Zn₂Al layered double hydroxides intercalated and adsorbed with anionic blue dyes: a physico-chemical characterization, *J. Colloid Interface Sci.* 333 (2009) 120–127.
- [30] L.Y. Liu, M. Pu, L. Yang, D.Q. Li, D.G. Evans, J. He, Experimental and theoretical study on the structure of acid orange 7-pillared layered double hydroxide, *Mater. Chem. Phys.* 106 (2007) 422–427.
- [31] S. Salleres, F.L. Arbeloa, V. Martínez, T. Arbeloa, I.L. Arbeloa, Photophysics of rhodamine 6G laser dye in ordered surfactant (C12TMA)/clay (laponite) hybrid films, *J. Phys. Chem. C* 113 (2009) 965–970.
- [32] F.L. Arbeloa, V.M. Martínez, Orientation of adsorbed dyes in the interlayer space of clays. 2. Fluorescence polarization of rhodamine 6G in laponite films, *Chem. Mater.* 18 (2006) 1407–1416.
- [33] H. Chai, Y.J. Lin, D.G. Evans, D.Q. Li, Synthesis and UV absorption properties of 2-naphthylamine-1,5-disulfonic acid intercalated Zn–Al layered double hydroxides, *Ind. Eng. Chem. Res.* 47 (2008) 2855–2860.
- [34] C. Li, L.Y. Wang, D.G. Evans, X. Duan, Thermal evolution and luminescence properties of Zn–Al-layered double hydroxides containing europium(III) complexes of ethylenediaminetetraacetate and nitrilotriacetate, *Ind. Eng. Chem. Res.* 48 (2009) 2162–2171.
- [35] Y. Kohno, K. Totsuka, S. Ikoma, K. Yoda, M. Shibata, R. Matsushima, Y. Tomita, Y. Maeda, K. Kobayashi, Photostability enhancement of anionic natural dye by intercalation into hydrotalcite, *J. Colloid Interface Sci.* 337 (2009) 117–121.
- [36] H. Hata, T.E. Mallouk, K. Kuroda, Color tuning of an acidic blue dye by intercalation into the basic interlayer galleries of a poly(allylamine)/synthetic fluoromica nanocomposite, *Chem. Mater.* 21 (2009) 985–993.
- [37] R. Marangoni, C. Taviot-Guého, A. Illaik, F. Wypych, F. Leroux, Organic inorganic dye filler for polymer: blue-coloured layered double hydroxides into polystyrene, *J. Colloid Interface Sci.* 326 (2008) 366–373.
- [38] R.M. Jones, T.S. Bergstedt, C.T. Buscher, D. McBranch, D. Whitten, Superquenching and its applications in J-aggregated cyanine polymers, *Langmuir* 17 (2001) 2568–2571.
- [39] P.J. Sideris, U.G. Nielsen, Z. Gan, C.P. Grey, Mg/Al ordering in layered double hydroxides revealed by multinuclear NMR spectroscopy, *Science* 321 (2008) 113–117.